Manipulation and Microrheology of Carbon Nanotubes with Laser-Induced Cavitation Bubbles

P. A. Quinto-Su, X. H. Huang, S. R. Gonzalez-Avila, T. Wu, and C. D. Ohl

Division of Physics and Applied Physics, School of Physical and Mathematical Sciences, Nanyang Technological University, Singapore 637371, Singapore

(Received 21 July 2009; revised manuscript received 10 November 2009; published 7 January 2010)

Multiwalled carbon nanotubes (MWCNT) are exposed to a transient and strong liquid jet flow created by a pair of differently sized laser-induced cavitation bubbles. The position and size of the bubbles are controlled with a spatial light modulator within a 15 μm thick liquid gap. Depending on the tube's position with respect to this jet flow, rotation, translation, and a bending deformation is observed with a high-speed camera recording at up to 300 000 frames per second. By measuring the decay time of the respective bending modes we determine the flexural rigidity of MWCNTs to be on the range of 0.45–4.06 $\times 10^{-19}$ N m^2. The average diameter of the MWCNTs is 117.8 $\pm$ 6.7 nm with a thickness of 4.6 $\pm$ 0.75 nm, yielding a Young's modulus between 0.033–0.292 TPa.

DOI: 10.1103/PhysRevLett.104.014501 PACS numbers: 47.55.D−, 42.40.Eq, 62.25.−g

Introduction.—Since the discovery of carbon nanotubes [1], the curiosity of the science of nanoscale entities as well as their potential applications in nanoelectromechanical devices [2] have stimulated several studies geared towards manipulation [3–6] and measuring their mechanical properties (rheology) [7–14]. However, due to the size of the nanotubes and nanorods, controlling and measuring their properties is a challenge. The manipulation of nanostructures is typically done in a liquid environment in order to avoid the attractive van der Waals interaction with surfaces. Because of the smallness of the devices the fluid regime is dominated by surface forces; i.e., manipulation of these structures occurs in a viscosity dominated and reversible Stokes' flow regime [3]. Several clever solutions for manipulating nanoscale objects have been shown, yet most are tailored to specific properties of the objects and involve the use of electric and or magnetic fields.

In this study we describe a new method to manipulate (translation and/or rotation) and to probe (deflection) nanotubes immersed in liquid. It involves a pair of laser-induced cavitation bubbles to actuate a liquid flow on very short spatial (μm) and temporal scales (μs), yet creating very high velocities. In this way, the nanotubes are displaced on a time scale shorter than 10 μs, at the same time the nanotubes are bent due to the differences in flow speeds across their length. By measuring the time it takes for the individual bending modes of the nanotube to recover its original shape we can estimate the flexural rigidity of the object $\kappa = EI$ where E is the bending modulus and I is the cross-sectional moment of inertia. This cavitation based technique has the advantage that it is independent of the material properties of the nanotubes and does not require microfabrication, only optical access.

Experimental setup.—An Nd:YAG laser generates a single pulse at a wavelength of 532 nm with a duration of 6 ns [Fig. 1(a)]. The beam propagates through a half wave plate to rotate the polarization and then through a telescope formed by lenses L_1 and L_2 to cover the display of the spatial light modulator (SLM). A digital hologram is projected on the SLM to create two foci [15,16]. The hologram on the SLM imparts the phases needed to obtain the desired pattern at the focal plane of the microscope objective, i.e., at its Fourier plane. This foci pattern is created within a thin liquid gap filled with ink. In this way at both laser foci a cavitation bubble is generated through linear absorption [15]. The nanotubes are imaged with a 60× water immersion microscope objective using an inverted microscope. The manipulation and the subsequent shape recovery of the nanotubes is recorded with a high-speed camera (Photron SA-1) at framing rates of up to 300 000 frames per second.

Liquid gap and geometry.—The sample is prepared using an essentially two-dimensional liquid gap filled with refill ink for inkjet printers (yellow, Maxtec). Its density and viscosity are similar to water (density $\rho = 1046 \pm 1$ kg/m^3 and dynamic viscosity of approximately 2 cP). The nanotube solution is previously mixed with the ink in a proportion of 1 to 3. The gap is created by sandwiching spacers with a height of 15 μm (in z) between two #1 microscope slides [Fig. 1(b)].

MWCNT preparation.—Anodic alumina membranes (AAM) were prepared by a two-step anodization process similar to the one reported in Ref. [17] and the MWCNT were synthesized within the AAM through chemical vapor deposition. The morphology of the array was characterized with a field emission scanning electron microscope (JEOL JSM-6700 F). The nanotubes have an average length of 16.3 $\pm$ 2.6 μm and outer diameters d_{ext} of 117.8 $\pm$ 6.7 nm with a wall thickness of 4.6 $\pm$ 0.75 nm, see Fig. 1(c).

Bubble dynamics.—The frames (a)–(c) of Fig. 2 depict the bubble pair recorded at 100 000 fps with a shutter time of 5.4 μs. The first frame, Fig. 2(a), is recorded 5 μs before the laser pulse arrives at the sample. The second frame, Fig. 2(b), is taken when the left bubble has reached about its maximum size, i.e., 5 μs after the arrival of the laser pulse. The bubble on the left is smaller and collapses

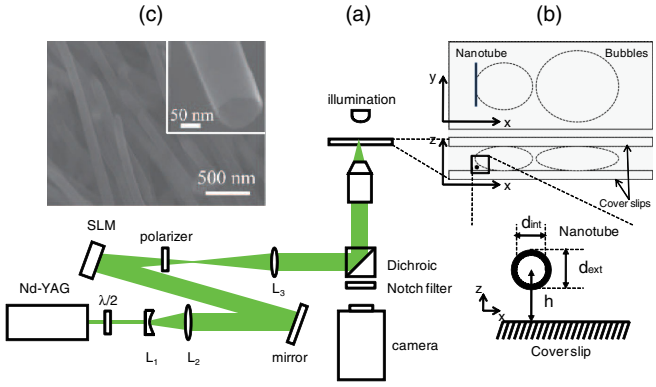

FIG. 1 (color online). Experimental setup and geometry: (a) optical path and equipment used. (b) Geometry of the liquid gap with the bubbles and the nanotube (not to scale). Upper inset: *xy* projection as imaged with the microscope objective. Middle inset: side view or *xz* projection. Lower inset: magnified view showing the relevant parameters for the nanotube, d_{ext} is the external diameter of the tube, d_{int} the internal diameter and h is the distance of the axis from the lower glass cover slip. (c) Multiwalled carbon nanotubes. Upper-left inset: scanning electron micrograph, showing the morphology of the MWCNTs.

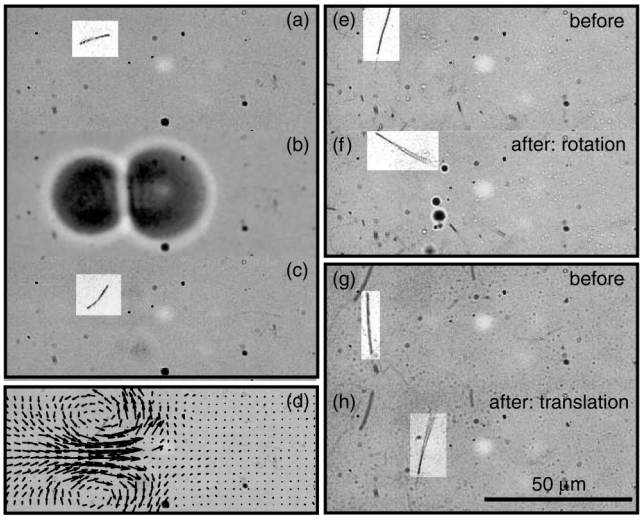

FIG. 2. Left column: Bubble dynamics for an uneven sized pair of bubbles, recorded at 100 000 frames per second, with an exposure time of 5.38 μs. The top three frames (a)–(c) show the interaction of the flow with a nanotube leading to its rotation. (d) Averaged flow field obtained with particle image velocimetry using two frame correlation: the first frame just after the larger bubble has collapsed and the second frame 10 μs later. The right column demonstrating nanotube manipulation: (e),(f) Sequence of pictures before and after cavitation resulting into a clockwise rotation of the nanotube. (g),(h) Sequence of nanotubes translating towards the right. Note that neighboring nanotubes are very little affected by the main flow.

first creating a strong jet towards the larger one along the line joining their centers, this jet flow can reach speeds of several tens of meters per second [18] and it is used to displace the nanotubes and to cause bending. Finally, frame (c) of Fig. 2 taken 10 μs after frame (b) is showing that both bubbles have collapsed within 15 μs after the arrival of the laser pulse. The maximum radius for the smaller and larger bubble is around 10 and 20 μm, respectively.

By measuring the displacement of 2 μm diameter tracer particles the general features of the flow a few micrometers from the glass coverslip are revealed as shown on Fig. 2(d). The basic flow is a high-speed jet pointing from the position of the smaller bubble to the larger bubble, here from left to right with a width of approximately 13 μm. Additionally, a stagnation point on the connecting line between the centers of the two bubbles exists which also forms a separatrix for the lower and upper recirculating flows. The flow is rather localized, and spans approximately a region within a radius of $\sim$30 μm around the stagnation point. The flow depicted on Fig. 2(d) is not the flow experienced by the nanotubes, it represents an averaged outer flow driving the boundary layer where the nanotubes are located [Fig. 1(b)]; i.e., we overestimate the velocities.

Next, we explain why a flow of this kind is generated. Upon collapse, bubbles can jet towards other bubbles or rigid boundaries [19–21]. In the case of differently sized bubbles the smaller bubble collapses first and because it is accelerated towards the larger bubble it develops a jet flow in the direction of the larger bubble. When the larger bubble collapses, the smaller bubble has already disintegrated and therefore the larger one does not anymore develop a jet flow. No further reexpansion of the first bubble is observed, likely due to the quasi-two-dimensional geometry which results in a milder collapse and therefore weaker acoustic emissions from the larger bubble.

Nanotube manipulation and interaction with the induced flow.—The directed flow field created by the bubble pair [Fig. 2(d)] is used for the manipulation of nanotubes. Because of viscosity, lateral momentum of the flow as depicted in Fig. 2(d) is transported downwards to the location of the nanotube. We observe that only during the lifetime of the smaller bubble the nanotubes are displaced (translated, rotated, or both). When the smaller bubble has collapsed the motion of the nanotube stops abruptly. Because of a strongly orientation dependent drag force typical for objects with a high aspect ratio [22–25] the fluid-structure interaction occurs preferably in the direction normal to the nanotube's contour. Thus, by changing the position and orientation of the jetting flow with respect to the nanotube, specific translation and/or rotation can be achieved. Figures 2(e) and 2(f) show the rotation of a nanotube imaged before and after cavitation. Before the creation of the bubbles, Fig. 2(e), the initial position of the nanotube is almost perpendicular to the line joining the centers of the bubbles but off center, so that the jet interacts more strongly with the lower portion of the nanotube and rotating it. In contrast in Fig. 2(g) the initial position of the nanotube is perpendicular to the line joining the centers of

the bubbles and nearly centered around the jet; that is why the object performs a translation towards the right, Fig. 2(h).

Nanotube bending.—While the nanotube interacts with the jet created by the cavitation bubbles it bends due to the difference in flow velocity across its length. Then, the nanotube starts to recover its original shape under the elastic restoring forces acting against the transverse hydrodynamic drag in a time scale of tens of microseconds. In all our experiments we have only observed planar bending. Estimates of the focal depth and measurements of the constancy of nanotube's contour length suggest a perfectly planar motion with less than 0.9 μm out of plane motion (xy) over the whole length. This allows us to model the shape recovery with the hydrodynamic beam equation [14,24–27]:

$$\kappa \frac{\partial^4 y}{\partial s^4} = -\gamma \frac{\partial y}{\partial t}. \tag{1}$$

The "deflection" of the nanotube is described by $y(s)$, where s is the contour length of the tube, γ is the drag coefficient, and $\kappa = EI$ is the flexural rigidity. The drag coefficient for motion perpendicular to the axis of the nanotube and parallel to the cover slip is $\gamma = 4\pi\eta/\cosh^{-1}(h/r)$ [23,24,28–30], where h is the distance of the axis from the surface and $r = d_{\text{ext}}/2$ is the outer radius of the nanotube [Fig. 1(c)]. The distance h is estimated as the electrical double layer thickness between the substrate and the nanotube surface. The Debye length κ_D^{-1} is $0.304/[1{:}1\,\text{electrolyte}]^{1/2}$, $0.176/[1{:}2\,\text{electrolyte}]^{1/2}$, and $0.152/[2{:}2\,\text{electrolyte}]^{1/2}$ nm, where notation [electrolyte] stands for the molar concentration for the respective type of electrolyte [31]. The Debye length is maximum for 1:1 electrolytes for a given concentration. Also, as the concentration increases the Debye length decreases. We estimate the maximum distance of the nanotube to the substrate by using the 1:1 electrolyte and an equilibrium H^+ ion concentration for carbon dioxide dissolved in pure water of 2.5×10^{-6} M [4] (as minimum concentration), then $\kappa_D^{-1} \sim 192$ nm. Assuming that the ink is a 2:2 electrolyte and the concentration the same, $\kappa_D^{-1} = 96$ nm. These assumptions are in agreement with a pH-level measurement of 5.7. Adding the outer radius of the nanotube, we estimate the upper bound for h (Fig. 1) to be in the range of 200 ± 50 nm. The solution for the hydrodynamic elastic Eq. (1) is given by $y_n(s,t) = a_n e^{-t/\tau_n} W_n(s,L)$, where the spatial part $W_n(s,L)$ satisfies the boundary conditions (BCs) for free ends [25,32] and has the form $W_n(s,L) = A\cos(q_n s/L) + B\sin(q_n s/L) + C\cosh(q_n s/L) + D\sinh(q_n s/L)$ [32]. The BC yields the coefficients for $W_n(s,L)$ [25] and the equation for solvability $\cos(q_n)\cosh(q_n) = 1$ that define the characteristic frequencies q_n. The first five values of q_n are 4.7301, 7.8533, 10.9957, 14.1372 and 17.2788. The shape $y(s,t)$ can be expressed as $y(s,t) = \sum_n y_n(s,t) = \sum_n a_n e^{-t/\tau_n} W_n(s,L)$, where $a_n = \frac{1}{G}\int_{s=0}^{s=L} y(s) W_n(L,s)ds$ and $G^2 = \int_{s=0}^{s=L} |W_n(L,s)|^2 ds$. Substituting the expression for $y_n(s,t)$ into Eq. (1) and solving for the flexural rigidity κ we obtain

$$\kappa = \gamma \frac{(L/q_n)^4}{\tau_n}. \tag{2}$$

The drag coefficient γ increases with decreasing h so that the upper bound that we estimated for h will yield a lower bound on the values for the flexural rigidity.

Measurement of elastic properties.—Figure 3 presents an example of the experiment to estimate the flexural rigidity of the nanotubes. Selected frames of a high-speed recording (250 000 fps) are shown on Fig. 3(a); the third frame displays the bent nanotube just after the collapse of the bubbles. Figure 3(b) shows the extracted shape from the high-speed recordings starting with the shape of the tube just after the bubbles collapsed (green, on top) till the final shape in red color (bottom). The amplitudes a_n of the first three modes are plotted as a function of time in Fig. 3(c) and are fitted to decaying exponentials. The flexural rigidity κ is extracted with Eq. (2) using the decay time of the first mode (τ_1), with the exception of the first run of nanotube 4, since modes higher than 2 have a negligible amplitude. Table I summarizes the results. For nanotubes numbered 1–4 the experiment is repeated sev-

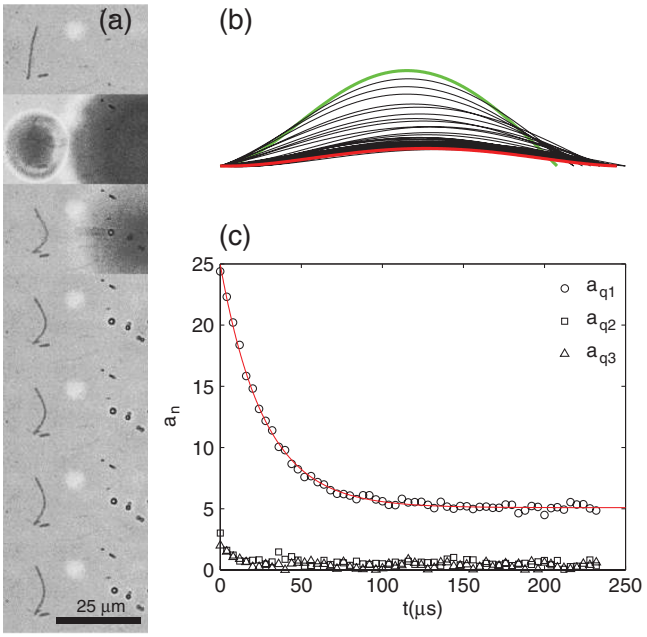

FIG. 3 (color online). Dynamics of the nanotube bending: (a) image sequence from top to bottom recorded at a rate of 250 000 frames per second (4 μs interframe time, movie available in Ref. [35]). (b) Shape of the nanotube as a function of time from the high-speed recording, starting from the deformed shape (green, on top) shown on the third frame of (a) just after the collapse of the bubbles and ending with the shape shown in red (bottom). (c) The amplitude of the first three modes a_n as a function of time, only the first mode is significant in describing the shape recovery. The solid line shows the fit to a decaying exponential with $\tau_1 = 27.06$ μs.

TABLE I. Values for κ and E calculated using Eq. (2) and a value for $h = 200 \pm 50$ nm. The errors correspond to the upper and lower values that arise from h.

nanotube	$L(\mu\text{m})$	$\tau_1(\mu\text{s})$	$\tau_2(\mu\text{s})$	$\kappa(\times 10^{-19}\ \text{N m}^2)$	E (TPa)
1	15.8	10.85	···	$1.52^{+0.29}_{-0.16}$	$0.109^{+0.021}_{-0.011}$
1	15.8	9.74	···	$1.68^{+0.33}_{-0.18}$	$0.121^{+0.023}_{-0.013}$
1	15.8	10.56	···	$1.56^{+0.30}_{-0.17}$	$0.112^{+0.022}_{-0.012}$
2	19	17.43	···	$1.97^{+0.38}_{-0.21}$	$0.141^{+0.027}_{-0.015}$
2	19	18.31	3.68	$1.88^{+0.36}_{-0.20}$	$0.135^{+0.026}_{-0.015}$
2	19	21.75	···	$1.58^{+0.30}_{-0.17}$	$0.113^{+0.022}_{-0.012}$
3	14.2	9.32	···	$1.17^{+0.23}_{-0.13}$	$0.084^{+0.016}_{-0.009}$
3	14.2	9.25	···	$1.18^{+0.23}_{-0.13}$	$0.085^{+0.016}_{-0.009}$
4	15.8	···	3.87	$0.57^{+0.11}_{-0.06}$	$0.041^{+0.008}_{-0.004}$
4	15.8	27.06	5.38	$0.61^{+0.12}_{-0.07}$	$0.044^{+0.008}_{-0.004}$
5	13.3	15.99	···	$0.51^{+0.10}_{-0.06}$	$0.037^{+0.007}_{-0.004}$
6	19.7	11.70	···	$3.41^{+0.65}_{-0.37}$	$0.245^{+0.047}_{-0.027}$

eral times. In all cases the extracted values for κ and E are repeatable. The values for the flexural rigidity have a range between 0.45 and 4.06×10^{-19} N m^2, while the Young's modulus ranges from 0.033 to 0.292 TPa. We explain the wide spread of moduli with the nonuniformity of the nanotubes, in particular with the variations in thickness and the presence of defects along their contour. The values for the Young's modulus that we obtain are similar to the values reported in literature [7,9,11,12,33] and in theoretical [34] studies of multiwalled carbon nanotubes. These studies report values between 0.1 and 0.6 TPa. Our method would be more accurate once we know the distance h of the nanotube from the surface to a higher precision. This might be achieved using confocal microscopy and fluorescent tagged nanotubes.

Summary.—Using the flow created by two unequally sized cavitation bubbles we can manipulate and probe individual nanotubes. This novel technique shares some of the advantages from optical tweezers, as it needs only optical access. Also, it is independent of the material properties of the nanotubes and generates forces that can bend individual nanotubes.

We acknowledge financial support through Nanyang Technological University (RG39/07) and The Ministry of Education (T208A1238), Singapore.

[1] S. Iijima, Nature (London) **354**, 56 (1991).
[2] P. Kim and C. M. Lieber, Science **286**, 2148 (1999).
[3] D. L. Fan, F. Q. Zhu, R. C. Cammarata, and C. L. Chien, Phys. Rev. Lett. **94**, 247208 (2005).
[4] B. Edwards, T. S. Mayer, and R. B. Bhiladvala, Nano Lett. **6**, 626 (2006).
[5] K. Keshoju, H. Xing, and L. Sun, Appl. Phys. Lett. **91**, 123114 (2007).
[6] D. Wang, R. Zhu, Z. Zhou, and X. Ye, Appl. Phys. Lett. **90**, 103110 (2007).
[7] M. F. Yu, O. Lourie, M. J. Dyer, K. Moloni, T. F. Kelly, and R. S. Ruoff, Science **287**, 637 (2000).
[8] E. W. Wong, P. E. Sheehan, and C. M. Lieber, Science **277**, 1971 (1997).
[9] R. Gao, Z. L. Wang, Z. Bai, W. A. de Heer, L. Dai, and M. Gao, Phys. Rev. Lett. **85**, 622 (2000).
[10] C. Ni, C. Deck, K. S. Vecchio, and P. R. Bandaru, Appl. Phys. Lett. **92**, 173106 (2008).
[11] M. M. J. Treacy, T. W. Ebbesen, and J. M. Gibson, Nature (London) **381**, 678 (1996).
[12] P. Poncharal, Z. L. Wang, D. Ugarte, and W. A. de Heer, Science **283**, 1513 (1999).
[13] B. Mickey and J. Howard, J. Cell Biol. **130**, 909 (1995).
[14] R. Everaers, F. Jülicher, A. Ajdari, and A. C. Maggs, Phys. Rev. Lett. **82**, 3717 (1999).
[15] P. A. Quinto-Su, V. Venugopalan, and C. D. Ohl, Opt. Express **16**, 18 964 (2008).
[16] P. A. Quinto-Su and C. D. Ohl, J. Fluid Mech. **633**, 425 (2009).
[17] X. H. Huang, G. H. Li, X. C. Dou, and L. Li, J. Appl. Phys. **105**, 084306 (2009).
[18] E. Zwaan, S. Le Gac, K. Tsuji, and C. D. Ohl, Phys. Rev. Lett. **98**, 254501 (2007).
[19] J. R. Blake, P. B. Robinson, A. Shima, and Y. Tomita, J. Fluid Mech. **255**, 707 (1993).
[20] W. Lauterborn and H. Bolle, J. Fluid Mech. **72**, 391 (1975).
[21] D. C. Gibson and J. R. Blake, Appl. Sci. Res. **38**, 215 (1982).
[22] G. K. Batchelor, *An Introduction to Fluid Dynamics* (Cambridge University Press, Cambridge, 1998).
[23] A. J. Hunt, F. Gittes, and J. Howard, Biophys. J. **67**, 766 (1994).
[24] M. E. Janson and M. Dogterom, Biophys. J. **87**, 2723 (2004).
[25] C. H. Wiggins, D. Riveline, A. Ott, and R. E. Goldstein, Biophys. J. **74**, 1043 (1998).
[26] F. Gittes, B. Mickey, J. Nettleton, and J. Howard, J. Cell Biol. **120**, 923 (1993).
[27] B. Obermayer and O. Hallatschek, Phys. Rev. Lett. **99**, 098302 (2007).
[28] D. J. Jeffrey and Y. Onishi, Q. J. Mech. Appl. Math. **34**, 129 (1981).
[29] D. F. Katz, J. R. Blake, and S. L. Paveri-Fontana, J. Fluid Mech. **72**, 529 (1975).
[30] T. Kim, E. Meyhöfer, and E. F. Hasselbrink, Biomed. Microdevices **9**, 501 (2007).
[31] J. Israelachvili, *Intermolecular and Surface Forces* (Academic Press, London, 1992), p. 228.
[32] L. D. Landau and E. M. Lifshitz, *Theory of Elasticity* (Pergamon Press, New York, 1986).
[33] M. F. Yu, B. S. Files, S. Arepalli, and R. S. Ruoff, Phys. Rev. Lett. **84**, 5552 (2000).
[34] G. Gao, T. Cagin, and W. A. Woddard III, Nanotechnology **9**, 184 (1998).
[35] See supplementary material at http://link.aps.org/supplemental/10.1103/PhysRevLett.104.014501 for a movie of the image sequence of the dynamics of the nanotube bending recorded at a rate of 250 000 frames per second.